JOURNAL OF PROPULSION AND POWER
Vol. 25, No. 3, May–June 2009

Shock-Tunnel Experiments with a Mach 12 Rectangular-to-Elliptical Shape-Transition Scramjet at Offdesign Conditions

Milinda V. Suraweera* and Michael K. Smart†
University of Queensland, Brisbane, Queensland 4072, Australia

DOI: 10.2514/1.37946

A shock-tunnel investigation of a scramjet with a rectangular-to-elliptical shape-transition inlet and an elliptical combustor has been conducted at conditions simulating flight at Mach 8.7. The inlet was designed using a quasi-streamline-tracing method to have a design point of Mach 12.0 and operation down to Mach 6.0. The elliptical combustor began with a rearward-facing step around its perimeter and was followed by a constant-area and diverging section. The flowpath was completed by a short thrust nozzle. Gaseous hydrogen fuel was injected either through multiple portholes on the intake, a series of 48 portholes on the rearward-facing step at the combustor entrance, or a combination of the two. All fueling configurations resulted in a positive thrust coefficient at equivalence ratios above 0.3 without the use of ignition aids. Fuel injection in the intake produced robust combustion and good internal thrust levels, but led to inlet unstart at fuel equivalence ratios above 0.61. Stable mixing-limited combustion was observed for fuel injection at the step at all fuel equivalence ratios up to 1.23. Combined intake and step injection was observed to have the best performance. These experimental results demonstrate that rectangular-to-elliptical shape-transition scramjets designed for access-to-space applications can operate efficiently at conditions below the design Mach number.

Nomenclature

A	=	area
D	=	drag, N
F	=	force, N
H	=	combustor entrance height, mm
L	=	length
M	=	Mach number
m_c	=	mass capture ratio
P	=	pressure, kPa
T	=	thrust, N
x	=	axial distance along the model, mm
γ	=	ratio of specific heats
ϕ	=	fuel equivalence ratio

Subscripts

s	=	static condition
st	=	nozzle stagnation condition
$t2$	=	pitot
1	=	inlet entrance condition
∞	=	flight condition or flight direction

Introduction

THE development of scramjet engines that are capable of operating at flight velocities equivalent to Mach 10 and beyond is vital if the dream of cheap access-to-space vehicles is to be realized. Many contemporary scramjet flowpath designs can only operate in a small Mach number envelope and also require complex variable-geometry intakes and boundary-layer bleed systems to function. Other problems still to be resolved are the high drag and heat loads associated with sustained-high-speed atmospheric flight. What is needed is the development of designs with all of these factors in mind to provide a high overall system performance. Scramjet engines with rectangular-to-elliptical shape-transition (REST) inlets and elliptical combustors address a number of these problems. The inlets have a fixed geometry and do not require boundary-layer bleed to operate efficiently, thus offering greater system simplicity. In comparison with planar geometries with the same combustor cross-sectional area, the reduced wetted areas of the elliptical cross sections translate to lower viscous drag and thermal loads. The rounded design also has greater structural efficiency, enabling a reduction in the structural weight needed to withstand operational loads. Additionally, the elliptical geometry reduces the detrimental effects of hypersonic corner flows. Finally, REST scramjets have been shown experimentally to have the capability to operate at offdesign conditions [1].

The design of scramjet engines for flight above Mach 10 requires attendance to some key physical phenomena, all related to the extremely high velocity of the flow through the combustor. The first is the increased local heat transfer and skin friction relative to lower speeds. The second is that mixing lengths of fuel and air are very long relative to lower-speed engines, requiring a lengthening of the combustor if a traditional fueling station in the combustor is used. Both of these effects combine to increase the integrated drag D and heat load of the engine. The third consequence of high combustor velocity is the reduced amount of energy addition from fuel relative to the kinetic energy of the air passing through the combustor. This reduction in energy ratio lowers the thrust T available to the engine designer as flight Mach numbers increase. As the net thrust of an engine is $\Delta F = T - D$, it is clear that scramjet operation becomes more problematic with increased Mach number.

Ground testing of scramjet engines at conditions equivalent to greater than Mach 10 can only be performed in impulse facilities such as shock tunnels and expansion tubes. Although significant amounts of direct connect and component testing have been reported in these facilities [2–4], the most well-reported complete engine tests were conducted by NASA in support of the Hyper-X Mach 10 flight [5]. The flight performance of this engine matched well with these

Presented as Paper 0100 at the 46th AIAA Aerospace Sciences Meeting and Exhibit, Reno, NV, 7–10 January 2008; received 8 April 2008; revision received 4 November 2008; accepted for publication 25 November 2008.

*Postdoctoral Research Fellow, Centre for Hypersonics, Division of Mechanical Engineering. Member AIAA.

†Professor, Centre for Hypersonics, Division of Mechanical Engineering. Senior Member AIAA.

ground tests, and it enabled cruise operation of the vehicle [6] (i.e., $\Delta F = D_{\text{vehicle}}$). However, one drawback of this engine was the need for an ignition aid in the form of the pyrophoric gas, silane, to maintain robust combustion of the gaseous hydrogen fuel [5]. Because of the high molecular weight of silane, its continuous use results in a significant degradation in the specific impulse of the engine.

The current study involves a REST scramjet designed for Mach 12, but with a planned operational range from Mach 6 to 12. It represents an attempt to examine operation of a hydrogen-fueled engine at greater than Mach 10, without the need for ignition aids. To accomplish this, both fuel injection in the inlet and behind a step are examined. As a first step toward determining the offdesign performance of this engine concept, experiments have been conducted at conditions simulating flight at Mach 8.7.

Mach 12 REST Scramjet Design Methodology

The Mach 12 REST scramjet engine of interest in this paper was designed as an exploratory flowpath to examine the viability of 3-D scramjets with elliptical combustors at Mach numbers of interest for access-to-space systems. In such a system, the usefulness of air-breathing propulsion is very dependent on the range over which it is operational. The current flowpath was therefore designed to have a desired flight envelope from Mach 6–12. Although actual operational range of this flowpath can only be determined by experiment, both the upper and lower limits for the design were carefully chosen. The lower limit of Mach 6 was set to be above the regime in which large changes in combustor area ratio are needed for efficient engine operation, whereas the upper limit of Mach 12 was set by the requirement for a fixed-geometry engine.

With regard to the detailed design of the flowpath, the inlet geometry was generated using the REST inlet design tools of [7], applied with a design flight Mach number of 12, assuming that the engine is installed on a vehicle with a forebody equivalent to a 6 deg wedge. The inlet contraction ratio was determined by the requirement for both the flight dynamic pressure and combustor entrance pressure to be 0.5 atm., and the length of the inlet was reduced until shock-wave/boundary-separation criteria were reached. The elliptical combustor was sized to conservatively allow for ample mixing of fuel and air, and a short thrust nozzle was added. Multiple injector configurations were included in the engine design to allow exploration of their respective performance at different conditions. The current tests are a first step toward determining how this fixed-geometry engine can be made to operate over a significant Mach number envelope.

Experimental Program

Experimental Model

The scramjet model used in the test program, shown in Fig. 1, was 1980 mm long and had a maximum width of 180 mm. The test model consisted of four components: a short forebody plate, a REST inlet, an elliptical combustor, and a generic elliptical nozzle. The forebody and inlet sections were 150 and 1062 mm long, respectively. The inlet had a total geometric contraction ratio of 6.61, an internal contraction ratio of 2.26, and a short isolator downstream of the throat. The 150-mm-wide frontal capture area of the inlet was 113 cm^2, and all leading edges (including the forebody plate) had radii of 0.7 mm. Intake injection was through three 4-mm-diam portholes angled at 45 deg to the local flow, at a downstream distance of 652 mm from the leading edge of the model. The portholes were sized using [8] to enable the fuel jets to penetrate through the inlet boundary layer to facilitate mixing in the mainstream flow of the engine. The aspect ratio of the elliptical cross section at the end of the inlet was 1.76. The inlet section was terminated by a 2.5 mm rearward-facing circumferential step (area ratio of 1.245) in which fuel could be injected through a set of 48 portholes, 1.5 mm in diameter, angled at 10 deg to the axis of the combustor. The step height was sized to be smaller than the local boundary-layer thickness to promote combustion of fuel within the boundary layer. Sonic injection was employed for both fuel stations and a fast-response solenoid valve was used to supply gaseous hydrogen fuel to either or both of the fueling stations.

A cross section of the test model along the symmetry plane is shown in Fig. 2 to illustrate both fueling stations in finer detail. The combustor entrance height immediately downstream of the step was $H = 40.3$ mm and was angled at 6 deg to the inlet axis to realign the local flow with the nominal flight direction. The combustor consisted of a constant-area section, 322 mm in length ($L/H = 8.0$), and a diverging section, 242 mm in length ($L/H = 6.0$) to an area ratio of 2.0 relative to the inlet throat. The angle of divergence was kept constant around the circumference at approximately 1.6 deg. The generic thrust nozzle was an elliptical cone with a 201 mm length and an area ratio of 4.0. The scramjet engine is shown mounted in the shock-tunnel test section along with the pitot probe used for the tests in Fig. 3.

The inlet was machined using a three-axis mill from a plastic material called NECURON® 651 [9], which has a density of 660 kg/m^3 and a yield strength of 30 MPa. Because of the complexity of the geometry, the inlet was machined in two halves and bonded together with epoxy adhesive. Fiberglass layers were applied to the external body of the inlet, aft of the leading edges, to provide additional structural strength. The combustor section was made in a similar manner to the inlet. The elliptical nozzle was manufactured with a glass-filled nylon material called CAPForm™ using a selective laser sintering (SLS) technique and was hand-finished. The fuel reservoirs and injectors were machined from aluminum and mild steel, respectively. The process of machining enabled a high manufacturing tolerance of ± 0.05 mm, whereas the SLS technique produced an acceptable precision level of ± 0.15 mm in the nozzle. The model survived the entire 64-shot test program intact.

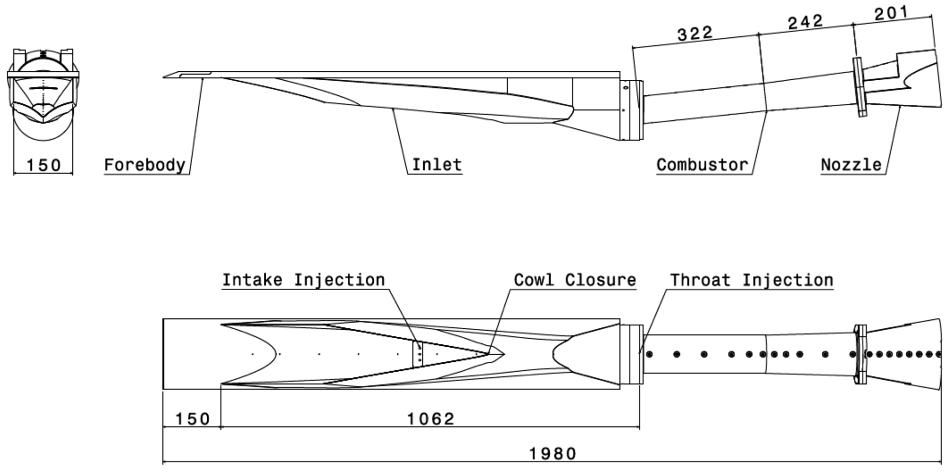

Fig. 1 Main components of the Mach 12 REST scramjet in the assembled test orientation.

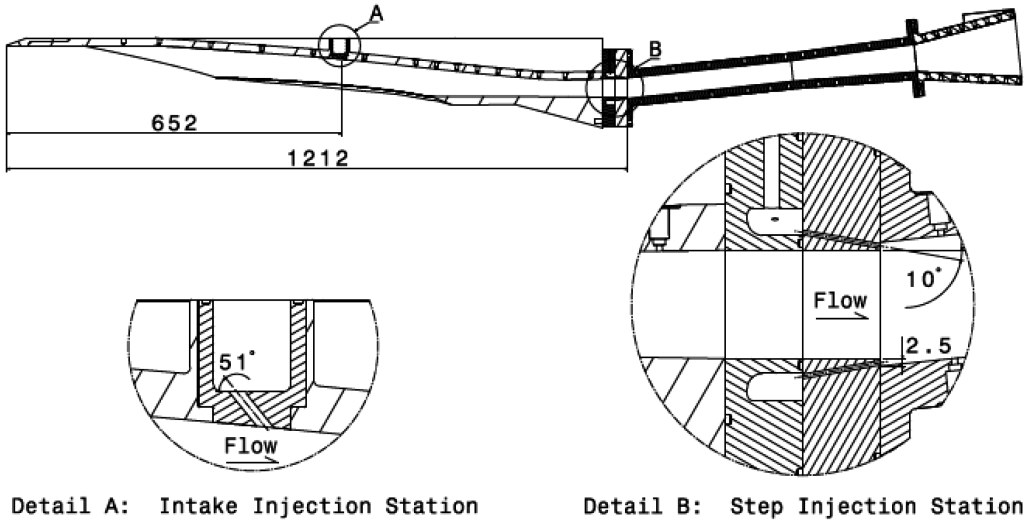

Fig. 2 Fueling stations of the Mach 12 REST scramjet.

Instrumentation, Fuel Supply, and Data Acquisition

The test surfaces comprised the intake wall and both the upper (body side) and lower (cowl side) sections of the combustor and nozzle. The centerline of each test surface was instrumented with Kulite™ series XTEL-190M pressure transducers at intervals ranging from 25 to 100 mm in length. Three pressure ranges were used in the test model: 0–68.8 kPa (0–10 psi), 0–172.3 kPa (0–25 psi), and 0–689.4 kPa (0–100 psi). The error associated with the use of these pressure transducers was $\pm 1.0\%$ of full scale. Both fuel plenum chambers were instrumented with two PCB model 111A26 piezoelectric pressure transducers. The error associated with the use of these pressure transducers was $\pm 2.0\%$ of full scale.

The fuel was injected from a room-temperature reservoir through a fast-acting solenoid valve. The fuel reservoir consisted of a coiled (14.19 m) Ludwieg tube that kept the temperature of the fuel approximately constant at 300 K during injection. An Asco Joucomatic solenoid valve, type SC B223A103, was used during the test program. A signal from a linear voltage displacement transducer, which measured the recoil of the shock tunnel, was used as a trigger for the fuel valve. Figure 4 shows typical time histories of the fuel plenum for the intake fuel injector and nozzle stagnation pressure during a fueled shot. Full-scale injection of the fuel flow was initiated at least 5 ms before test-flow arrival. During the experimental campaign, the plenum supply pressures were observed to be constant to within $\pm 2\%$ of the measured mean level during the test time. Each fueling configuration was calibrated before testing to determine the mass flow rate of hydrogen as a function of fuel plenum pressure. A 12-bit transient digital data acquisition and storage unit with a sampling time of 1 μs was used to record the data sets. The output of the majority of the pressure transducers was recorded through 4 multiplexers, resulting in an overall sampling frequency of 250 kHz per channel.

Facility and Test Conditions

The experiments were carried out in the University of Queensland's T4 free-piston reflected-shock tunnel [10]. The facility has a 229-mm-diam driver that is 26 m in length and a 75-mm-diam shock tube that is 10 m in length. A series of contoured axisymmetric nozzles are available for use over a wide range of hypervelocity conditions of interest to scramjet designers. A Mach 7.6 nozzle with a throat diameter of 16 mm and an exit diameter of 270 mm (area ratio of 150) was used for these experiments to simulate flight in the atmosphere at Mach 8.7 and at a dynamic pressure of 0.5 atm. Because of size limitations of the facility, the experiments were conducted in semi-free-jet mode, with the facility nozzle supplying airflow to the engine, assuming a precompression shock generated by a 6 deg two-dimensional forebody. A pitot-rake survey was initially performed to characterize the nozzle flow at locations of 75, 180, and 500 mm downstream of the nozzle-exit plane. Figure 5 shows the contours of experimental pitot pressure normalized by nozzle stagnation pressure at the 500 mm measurement plane (which is the approximate axial position of the inlet closure point for the tests), with the capture area of the inlet superimposed. These measurements indicate that relatively uniform flow enters the capture area of the engine.

Figure 6 shows typical nozzle stagnation, pitot, and static pressure traces for the test program. To facilitate comparison of time histories in Fig. 6, time delays of 304 and -278 μs were added to the time bases of the nozzle stagnation and static pressure traces, respectively, to account for the time taken for the test flow to traverse the distance

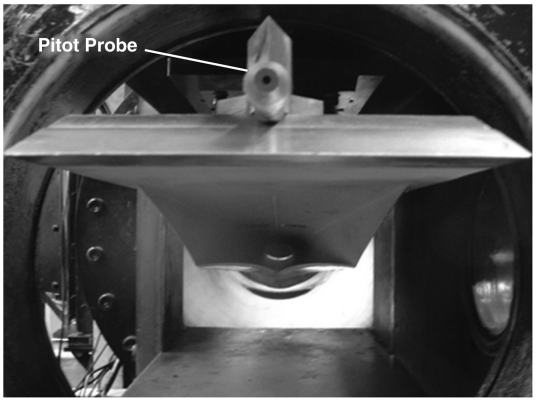

Fig. 3 Front view of the Mach 12 REST scramjet mounted in the T4 shock-tunnel test section.

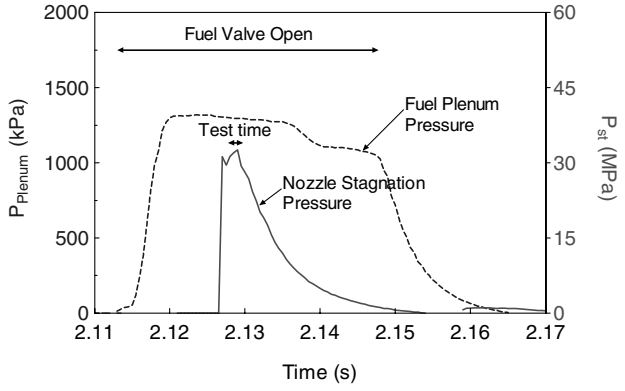

Fig. 4 Typical intake fuel plenum and nozzle stagnation pressure measurements.

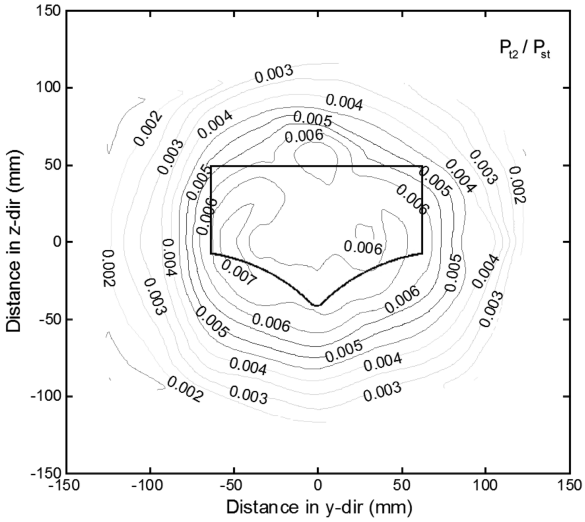

Fig. 5 Normalized pitot pressure contours (P_{t2}/P_{st}) 500 mm downstream of the facility nozzle exit (engine capture shown).

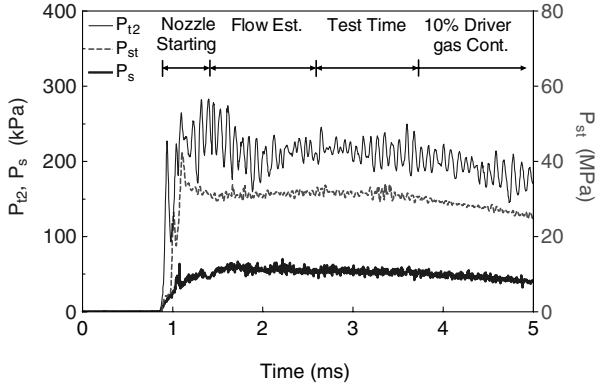

Fig. 6 Typical nozzle stagnation, pitot, and static pressure traces during the test program.

from the nozzle-supply (stagnation) region to the pitot probe and from the pitot probe to the static pressure tap. The beginning of the test time for the static pressure location is dependent on the nozzle starting process and the model flow-establishment time. The nozzle starting process is initiated by the rupture of the secondary diaphragm at the nozzle throat and is completed when the unsteady starting expansion is swept out of the nozzle and the boundary layers on the nozzle wall are fully established [11]. For the T4 shock tunnel, the onset of steady nozzle flow is taken to be the point in time when the ratio of the pitot pressure to stagnation pressure has reached a steady level.

Once the nozzle startup has been achieved, the test flow must have sufficient time to fully establish. The establishment time is the time required for the flow to reach steady state after flow onset. Past experimental and numerical studies for flat plates in shock-tunnel flows have correlated measurements for establishment time in terms of the number of model flow lengths [12–14]. Attached laminar and turbulent boundary layers take approximately 3.3 and 2.0 flow lengths, respectively, to reach steady state. As the boundary layers on the engine test surfaces were expected to be mainly turbulent for the present study, a value of 3.0 local flow lengths was considered to be sufficient for full flow establishment within the model. The end of the test time was dictated by either an unacceptable pressure decline in the flow (due to the arrival of expansion waves as a result of main diaphragm rupture) or by driver-gas contamination. In the current experiments, the end of test time was taken to be either when the pitot pressure dropped 10% below the mean level during the test period or when the level of driver-gas contamination in the test section exceeded 10% (whichever was shorter). Mass-spectrometry measurements of T4 shock-tunnel flow conditions obtained by Skinner [15], together with results from a driver-gas detector study [16], enabled the termination of the test time to be determined. For the nominal condition used in this study, this was approximately 2.9 ms after the onset of flow.

Table 1 lists the simulated flight conditions for the test program. In the semi-free-jet mode of these experiments, the nozzle-exit flow is considered to be equivalent to the forebody conditions, also listed in Table 1. These were calculated using a quasi-1-D nonequilibrium nozzle flow computer code [17] that was run with an expansion ratio that was consistent with the average measured ratio of P_{t2}/P_{st} within the capture area. Natural test-flow transition was assumed to have occurred approximately 150 mm upstream of the intake fueling station, in accordance with a previous flat-plate [18] study that determined that the transition unit Reynolds number for the shock-tunnel facility was approximately 2.0×10^6 m^{-1}.

Numerical Simulation of Fuel-Off Conditions

Numerical simulation of the engine flowpath with no fuel injection was carried out using the NASA Langley Research Center code VULCAN [19]. This code solves the three-dimensional Navier–Stokes equations for turbulent nonequilibrium chemically reacting flows using structured grids. A k-ω model was used to model the turbulent flow with transition specified at all leading edges. Figure 7 shows the calculated pressure contours in the symmetry plane of the scramjet engine with no fuel injection, assuming uniform inflow at the nominal experimental conditions. The vertical axis was increased in scale to aid visualization. At this offdesign condition, the inlet shock forms upstream of the cowl closure point of the inlet and the cowl shock strikes the body-side surface upstream of the throat. The subsequent return shock strikes the cowl-side surface upstream of the step, and a series of shocks and expansions traverse the flow in the combustor. The mass capture ratio for the inlet was calculated from this simulation to be $m_c = 91.9\%$ at this offdesign condition. This numerical solution is used in the paper to make a comparison with measured pressure distributions and to estimate the inlet and viscous drag on the engine.

Results and Discussion

Shock-tunnel tests were conducted to ascertain the performance of the scramjet engine over a range of fuel equivalence ratios. Three

Table 1 Nominal test-flow condition

Quantity	Units	Exp. error, %	Region	
			Simulated flight	Forebody/nozzle exit
Stagnation enthalpy	MJ · kg^{-1}	±8	4.18	4.18
Mach no.	——	±5	8.73	7.15
Static temperature	K	±12	256	371
Static pressure	kPa	±5	0.995	3.307
Dynamic pressure	kPa	±13	52.77	117.96
Static density	kg · m^{-3}	±11	0.0135	0.0310
Velocity	m · s^{-1}	±5	2795	2759
Unit length Reynolds no.	m^{-1}	——	2.32×10^6	3.97×10^6

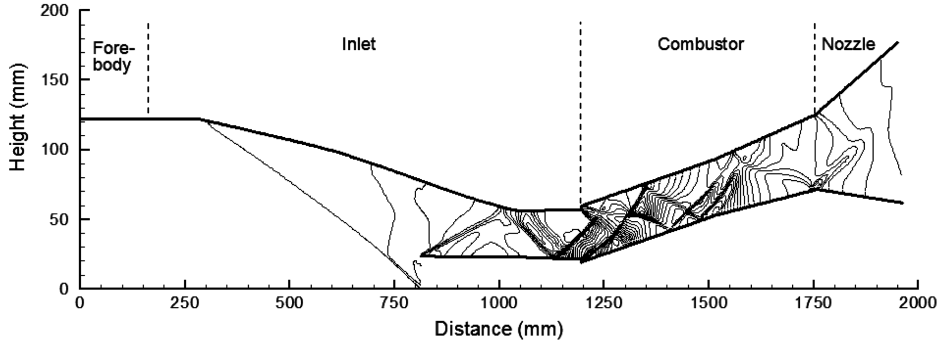

Fig. 7 Symmetry-plane pressure contours calculated from numerical simulations of the Mach 12 REST scramjet with no fuel addition.

categories of test were carried out: 1) with air as the test gas and no fuel injection (fuel off), 2) with air as the test gas and hydrogen fuel injection, and 3) with nitrogen as the test gas and hydrogen fuel injection (suppressed combustion). The differences between tests 2 and 3 were used to determine the effects of combustion, and the differences between tests 1 and 3 were used to determine the effects of fuel mass addition. Hydrogen fuel was injected at equivalence ratios between 0.30 and 1.23 using four distinct injection schemes. An initial study was conducted with the intake fuel injection scheme. This was followed by a study of injection from the step at the start of the combustor. Finally, two combined injection configurations using both fueling stations were employed. For the second combined configuration, the mass flow rate to the intake fueling station was reduced by placing a restrictor plate in the intake fuel line. The approximate ratios of mass flow rate through the intake and step fueling stations for the first and second combined injection schemes were 9:11 and 1:2, respectively.

Fuel-Off Results

The measured pressure distributions on the body-side and cowl-side test surfaces for an unfueled experimental run, along with numerical predictions, are shown in Fig. 8. Each pressure measurement represents a mean value of the pressure–time history during the test time. The static pressure measurements were normalized by the measured nozzle stagnation pressure for the test run (to account for run-to-run variations) and then multiplied by the nominal condition pressure ratio $\bar{P}_{st}/\bar{P}_1$ so that numerical values were relative to the nominal static pressure entering the engine. The label p/p_1 is used throughout the paper for these normalized pressures. To aid the physical interpretation of the static pressure data, the distribution of cross-sectional area through the scramjet module is also shown. The error bars in Fig. 8 were determined from the root sum square of the uncertainties in static pressure measurements and calculated stagnation pressure. These error bars are typical for the test program and, for clarity, are not included in later plots.

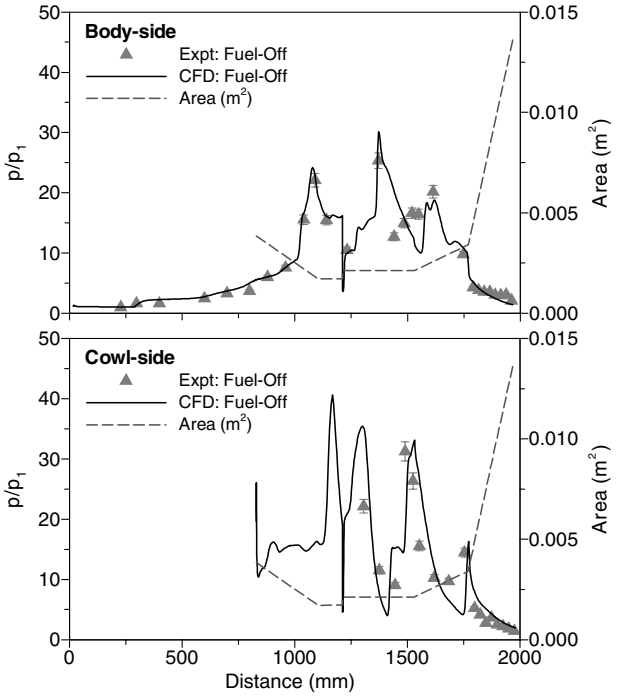

Fig. 8 Comparison between experimental and numerical prediction of surface pressure distributions with no fuel injection.

The fuel-off data show a gradual increase in pressure on the body side of the inlet until the throat, a slight drop in pressure immediately downstream of the step, a distinct shock-dominated flow structure on both the body and cowl sides in the combustor, and decreasing pressure levels along the nozzle section. These characteristics are all indicative of an engine flowpath that has started and an inflow boundary layer that transitions well upstream of the high-pressure region of the inlet. For the most part, the trend and the magnitude of the pressure levels measured in the experiment are matched closely by the numerical simulations for both the body-side and cowl-side test surfaces, within experimental uncertainty. However, on the body-side test surface of the combustor there is some disparity in the region $x = 1440$–1520 mm, and numerical results slightly overpredict the pressure levels on the cowl side of the nozzle. Overall, the good agreement between simulation and experiment gives some confidence that the flow entering the engine was close to the nominal test conditions and that the engine was aligned correctly in the tunnel.

Intake Fuel Injection Results

A set of normalized experimental pressure distributions along the body-side and cowl-side test surfaces is displayed in Figs. 9a and 9b for intake fuel injection at equivalence ratios of 0.30 and 0.41, respectively. These distributions are compared with a suppressed-combustion run at an equivalence ratio of 0.34 and a fuel-off shot. The suppressed-combustion data showed that fuel mass addition slightly increased the measured pressure levels in the latter part of the inlet. For the fuel-into-air data, both equivalence ratios showed pressure rise due to combustion upstream of the step on the body side of the model. At $\phi = 0.30$, fuel combustion had an effect from approximately $x = 1090$ mm, whereas for $\phi = 0.41$ the effect of combustion moved upstream to approximately $x = 1000$ mm. In contrast, the combustion-induced pressure rise remained downstream of the step on the cowl side, indicating that fuel injection on the body side of the intake does not penetrate to the cowl side. For both fuel conditions, sustained supersonic combustion is evident throughout the combustion-chamber section. The increase in measured pressure levels due to combustion is greater for $\phi = 0.41$, with a maximum pressure level of $p/p_1 \sim 60$. For $\phi = 0.30$, the significant rise in pressure at the entrance to the isolator is due to ignition and combustion of fuel. The larger increase in pressure in the isolator for $\phi = 0.41$ is attributed to local flow separation, as a result of the coupled effects of combustion-induced pressure rise and cowl shock interaction with the body-side boundary layer. Test runs conducted with intake injection at higher equivalence ratios of 0.62 and 1.03 resulted in the engine unstarting. This was indicated by a

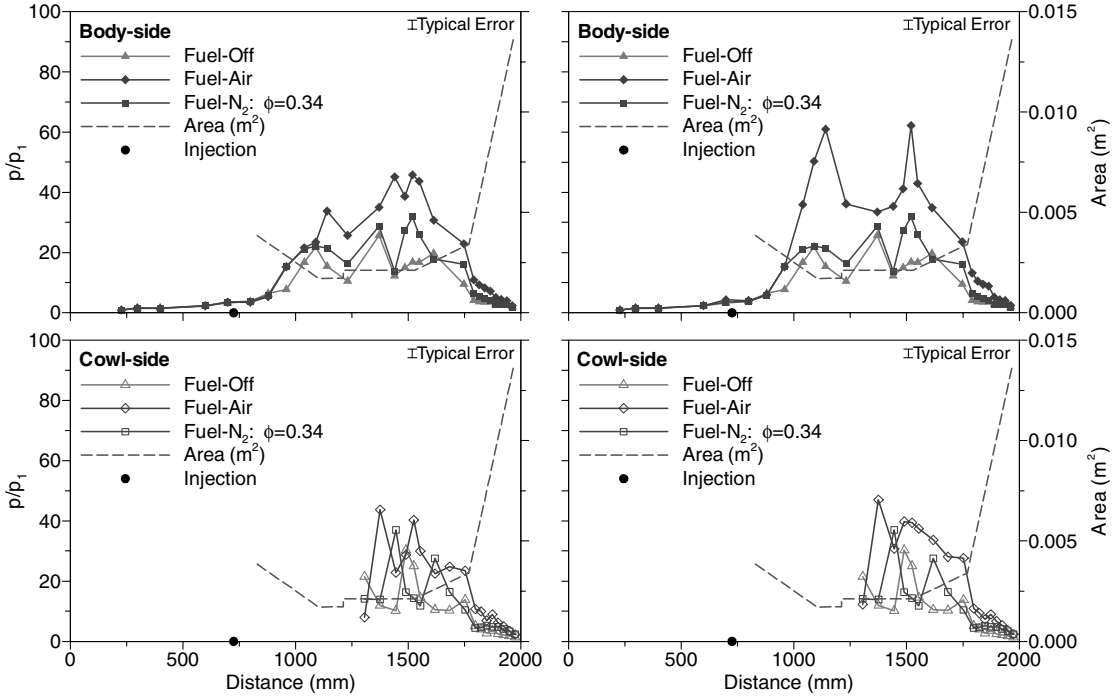

a) $\phi = 0.30$ b) $\phi = 0.41$

Fig. 9 Test-surface pressure distributions for intake injection.

large transient pressure rise originating in the isolator and moving toward the cowl closure location during the test time. This pressure spike was immediately followed by a sudden decrease in pressure inside the engine, indicating flow spillage. The upper limit for normal engine operation with intake injection was therefore between $\phi =$ 0.41 and 0.62.

Step Fuel Injection Results

Experiments with fuel injection at the step were conducted at equivalence ratios between 0.23 and 1.14. Measured pressure distributions along the body-side and cowl-side test surfaces are shown in Figs. 10 and 11. Figure 10 shows data for equivalence ratios of 0.23 and 0.53 in comparison with a suppressed-combustion run conducted at an equivalence ratio of 1.14 and a fuel-off shot. For both equivalence ratios, the suppressed-combustion data showed slightly increased pressure levels on the body-side test surface and changed the shock structure on the cowl-side test surface. The fuel-into-air data indicated that even at these low equivalence ratios, healthy combustion-generated pressure rise is occurring.

Typical pressure distributions for fuel into air at $\phi = 0.85$ and 1.14 are shown in Figs. 11a and 11b, respectively. Pressure distributions for both fuel cases are similar in trend and magnitude with

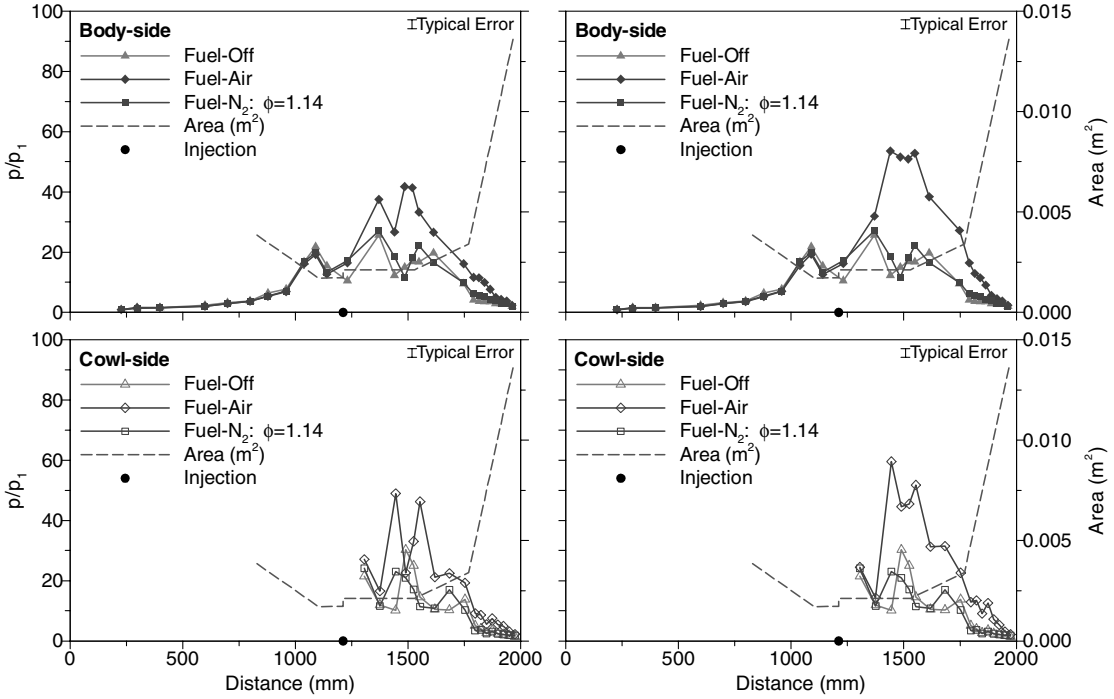

a) $\mu = 0.23$ b) $\phi = 0.53$

Fig. 10 Test-surface pressure distributions for fuel injection at step.

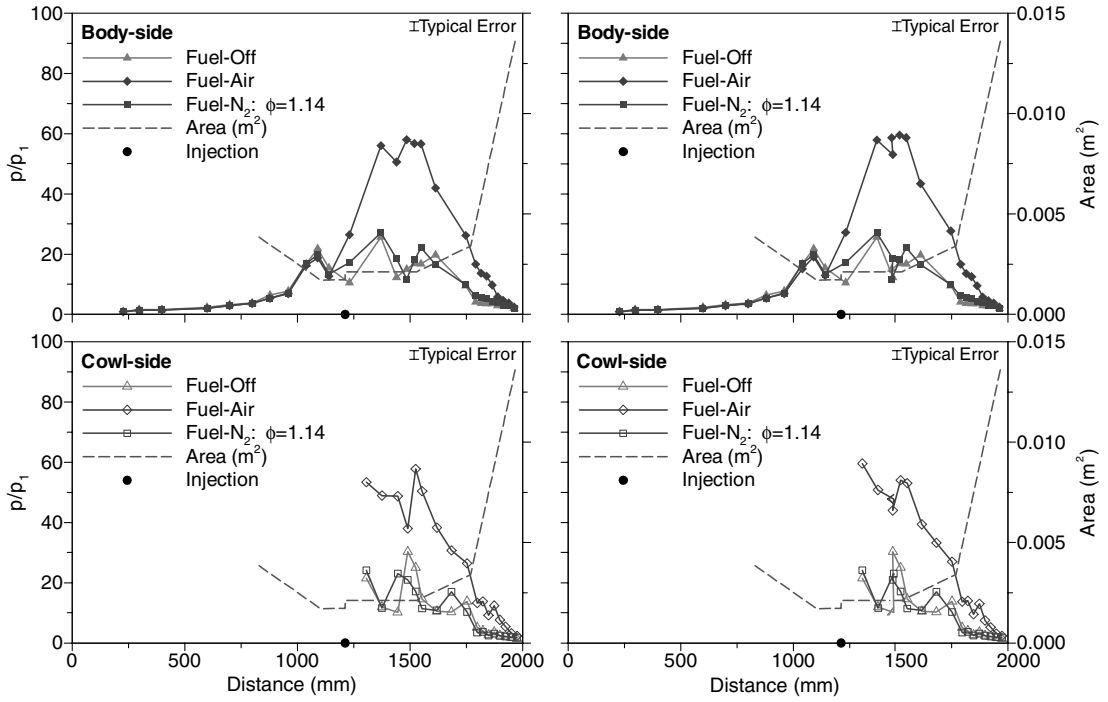

a) $\phi = 0.85$ b) $\phi = 1.14$

Fig. 11 Test-surface pressure distributions for fuel injection at step.

combustion-generated pressure rise downstream of the step. The pressure data on both the body- and cowl-side test surfaces indicate that robust burning occurred within the combustion chamber, with similar peak pressure levels on either side. Furthermore, peak pressure rise due to combustion occurred at the end of the constant-area section of the combustor for all step-injection test runs. A maximum pressure rise of $p/p_1 \sim 67$ was measured at $\phi = 1.14$, and fuel injection at the step never resulted in an inlet unstart.

Combined Fuel Injection Results

Pressure distributions for test runs using the combined 9:11 fuel injection scheme are shown in Fig. 12. Combustion runs at fuel equivalence ratios of 0.66, 1.02, and 1.23 are shown. One suppressed-combustion run was also conducted at an equivalence ratio of 1.23, for comparison. The pressure distributions show that significant combustion is taking place within the combustion chamber for all equivalence ratios tested with this injection scheme and that there is pressure rise due to combustion occurring upstream of the step. Note that at the higher equivalence ratios of 1.02 and 1.23, of which approximately 0.46 and 0.56, respectively, is injected in the intake, pressure levels along the isolator were stable and the engine showed no sign of unstarting. This was somewhat unexpected, as test runs conducted with intake injection alone produced engine unstart at an equivalence ratio between 0.41 and 0.62. Peak pressure rise due to combustion occurred at the downstream end of the constant-area

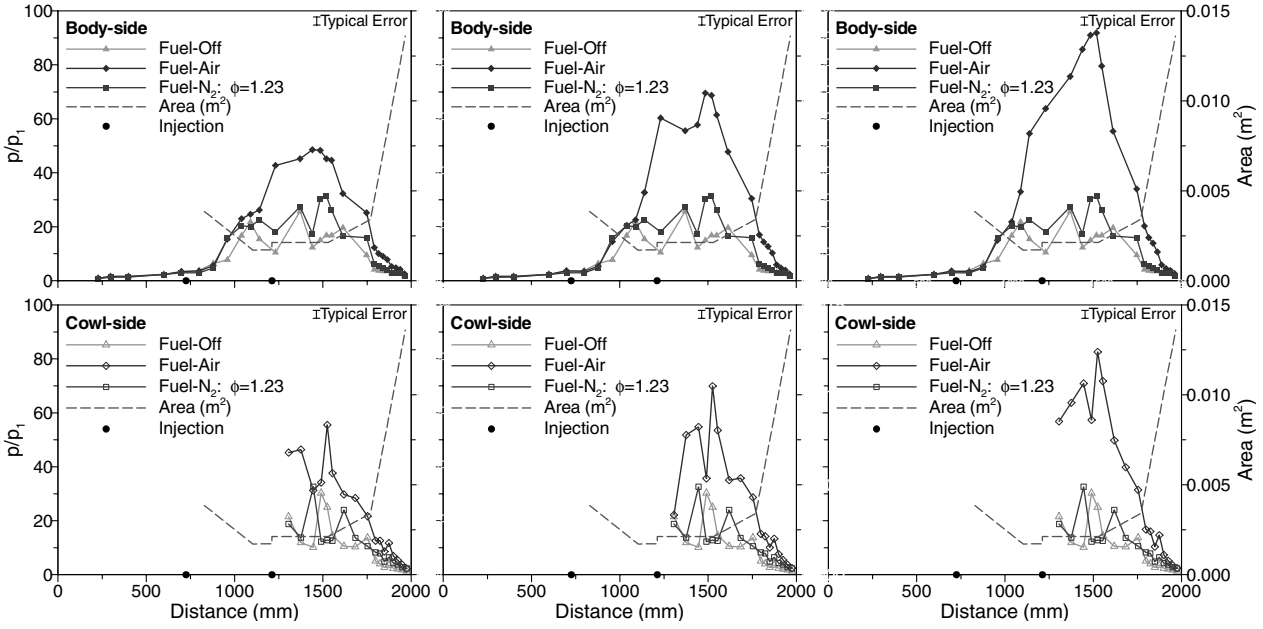

a) $\phi = 0.66$ b) $\phi = 1.02$ c) $\phi = 1.23$

Fig. 12 Test-surface pressure distributions for combined (9:11) injection.

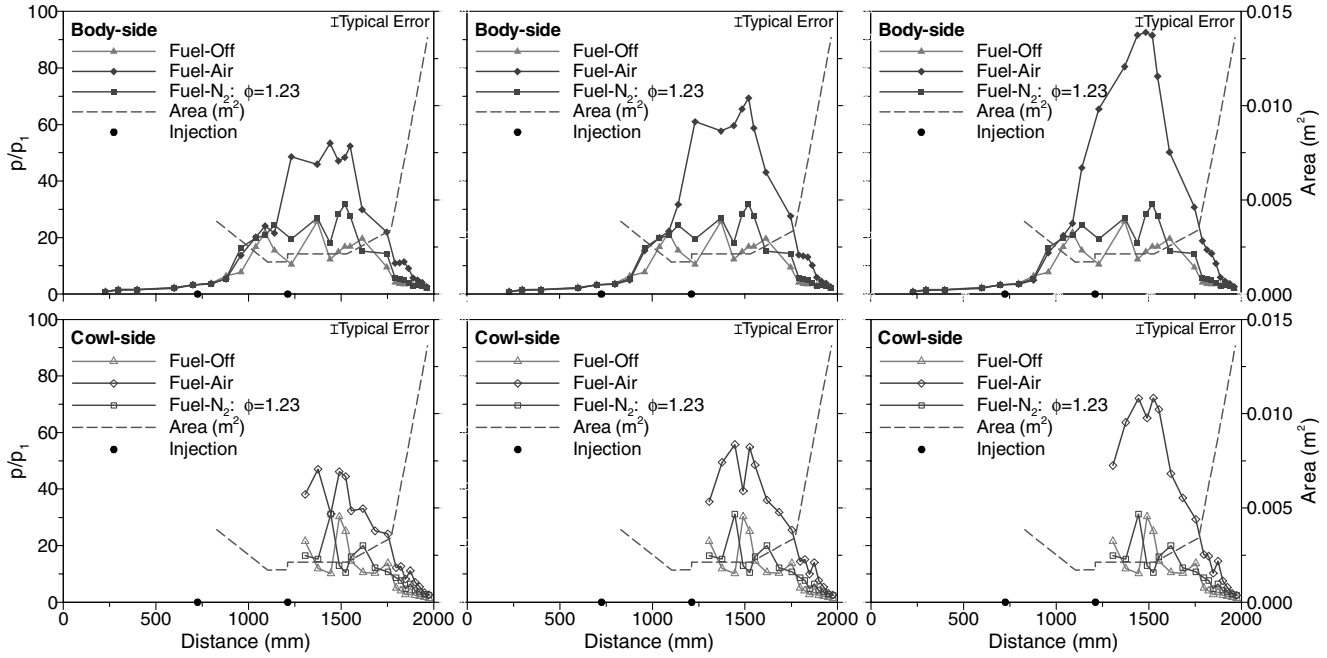

Fig. 13 Test-surface pressure distributions for combined (1:2) injection.

section of the combustor for all combined 9:11 injection test runs, with a maximum measured pressure rise of $p/p_1 \sim 108$ at $\phi = 1.23$. No inlet unstarts were observed for this fuel injection configuration.

Pressure distributions for test runs employing the combined 1:2 fuel injection scheme are presented in Fig. 13. For this injection scheme, combustion runs at fuel equivalence ratios of 0.64, 1.02, and 1.23 are shown. As before, one suppressed-combustion run was conducted at an equivalence ratio of 1.23 for a general comparison. The combined 1:2 fuel injection design was introduced to reduce the proportion of fuel injected in the intake, thereby reducing pressure levels within the inlet and isolator. It can clearly be seen that for all equivalence ratios, the measured pressure levels within the isolator are lower than those levels measured using the combined 9:11 injection scheme with the same overall equivalence ratio. At $\phi = 0.64$, pressure rise does not take place until the combustor entrance. For $\phi = 1.02$, however, there is very little pressure rise until immediately upstream of the step at approximately $x=$ 1140 mm. At $\phi = 1.23$, combustion-induced pressure rise is also limited to the region immediately upstream of the step and is at a significantly lower level than the corresponding equivalence ratio test run conducted with the 9:11 injection scheme. As with the earlier combined injection scheme, the pressure distributions show that significant combustion is taking place within the combustor, with particularly vigorous burning occurring at $\phi = 1.23$. Once again, peak pressure rise as a result of combustion occurs at the downstream end of the constant-area section of the combustor for all combined 1:2 injection test runs, with a maximum measured pressure rise of $p/p_1 \sim 113$ at $\phi = 1.23$. No inlet unstarts were observed for this fuel injection configuration.

It is clear from the presented pressure distributions that good combustion of hydrogen fuel is occurring in these experiments without the need for ignition aids, such as silane, or devices to add energy to the flow, such as plasma torches. This indicates that both intake injection and tangential injection behind a small step lead to robust fluid-dynamic flameholding in this flowpath at conditions simulating Mach 8.7 flight.

Calculated Engine Thrust Coefficients

Estimates of the internal thrust coefficient for the engine are shown in Fig. 14 as a function of equivalence ratio for all fuel injection configurations. These results represent the thrust potential of the flowpath, as the elliptical thrust nozzle is a simplified geometry and not representative of a practical configuration. Each thrust coefficient was calculated using the relation

$$C_T = \frac{F_\infty}{q_\infty A_\infty m_c} \tag{1}$$

where F_∞ is the summation of the internal forces on the engine in the flight direction, A_∞ is the area of the 100%-freestream-capture stream tube, and q_∞ is the dynamic pressure for the flight condition.

Because of limitations on the number and type of instruments installed in the engine, a combination of experimental pressure measurements and computational fluid dynamics (CFD) was used to determine F_∞. Pressure forces on the combustor and nozzle sections of the model were determined using the experimental pressure measurements, suitably integrated over the surface area. Furthermore, the thrust generated at the step was determined by the product of the step area (excluding the injection holes) and the average of the pressure levels measured at the first body- and cowl-side taps in the combustor. Because of the sparse nature of the pressure instrumentation in the inlet and isolator, however, the no-fuel numerical-simulation results were used to determine the pressure drag on these sections of the engine. This methodology was considered to supply a suitable approximation of the inlet drag, due to the good agreement between experimental and numerical pressure distributions shown in Fig. 8. The only caveats are the lack of accounting for 1) any increased inlet drag associated with pressure increases in the inlet from intake fuel injection and 2) any increased thrust due to combustion-generated pressure rise entering the slightly expanding isolator. To address caveat 1, an upper bound on the increased inlet drag was obtained by applying the pressure increase on the inlet measured for intake fuel injection at $\phi = 0.41$ (Fig. 9b) around the entire circumference of the inlet at the axial station of the pressure measurements. Because of the small frontal area associated with these surfaces, this upper bound amounted to a 2% increase in inlet drag. Furthermore, this increased inlet drag was opposed by combustion-generated pressure rise in the isolator (i.e., caveat 2). Therefore, for the purposes of the thrust estimates presented in this work, both caveats 1 and 2 were neglected.

No measurements of surface shear stress were taken during the experiments. In the absence of these measurements, viscous forces on the engine model for fuel-off and fuel-on operation were estimated using the no-fuel numerical results. The rationale for this is

based on the experiments of Tanno et al. [20], which found that estimates of fuel-off viscous drag in a scramjet could be used to predict overall fuel-on thrust measurements with supersonic combustion present. Furthermore, experiments by Goyne et al. [21] found that hypervelocity skin-friction drag levels were largely unaffected by combustion through tangential injection using a central strut. Based on these previous studies and in the absence of fuel-on numerical simulations, the use of no-fuel numerical results to estimate all viscous forces was considered to be reasonable for this exploratory study.

The thrust coefficient calculated for the internal flowpath without fuel injection was −0.13. Fuel mass addition in the combustion-suppressed test runs improved C_T to a peak level of −0.08 for $\phi = 1.23$ in both combined injection schemes. A key result of these experiments is that, as indicated in Fig. 14, all injection configurations generated positive net thrust from combustion at equivalence ratios of 0.3 and greater. Each fueling configuration exhibited different characteristics as equivalence ratio was increased. At equivalence ratios below 0.5, intake injection generated a linear increase in C_T that was higher than that produced by step injection for the same equivalence ratio. However, as the inlet unstarted at an equivalence ratio of less than 0.62, intake injection alone had its limitations for this engine.

The leveling off of thrust produced by step injection as equivalence ratios increase above 0.5 suggests that the combustion process was mixing-limited for this configuration. Nevertheless, step injection did produce approximately 30% more thrust than either combined injection scheme at the midrange equivalence ratios of 0.6–0.8. As equivalence ratios increased beyond 0.8, the combined injection configurations yielded the most thrust. This was attributed to the premixing enabled by intake injection and therefore to greater mixing and combustion efficiencies than with injection solely from the step. Within experimental uncertainty, the thrust produced by either combined injection scheme between $\phi = 0.64$ and 1.23 was the same. However, the combined 1:2 injection configuration is preferred due to the reduced levels of pressure rise within the isolator. At $\phi = 1.23$, at least 25% more thrust was generated using the combined injection schemes over the trend of the step-injection configuration.

Thrust Estimates with Skin-Friction Reduction

The geometry of the fuel injection station at the step was designed to promote skin-friction reduction in the combustor from boundary-layer combustion. Although the presence of skin-friction reduction cannot be confirmed in these experiments due to the lack of shear-stress instrumentation, it is of interest to examine what effect it could have on the overall thrust if it did occur. The flow phenomena that reduce skin friction through combustion are still the source of some debate; however, most sources (e.g., [22,23]) agree that the density reduction due to heat release at the surface results in local fluid dilatation that increases boundary-layer displacement. The expansion of the boundary layer reduces mean velocity gradients and hence lowers skin-friction levels. For the current experiments, the possible reduction in hypersonic turbulent skin friction by boundary-layer combustion of hydrogen was predicted using the model developed by Stalker [23] from the semi-empirical theory of Van Driest [24]. Estimates of thrust coefficient for step and combined fuel injection cases using the skin-friction-reduction model indicate that overall thrust coefficient for injection at the step is significantly higher than intake injection. In fact, the overall gain in thrust produced by step injection increased by at least 50% over values at which viscous drag reduction was not taken into account. For the combined injection schemes, these calculations indicate an increase in net thrust of at least 35%. Determination of the presence of this phenomenon will be the subject of future experiments using a thrust balance.

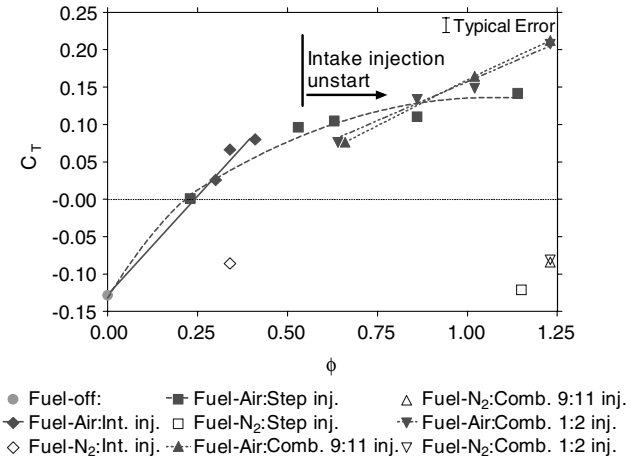

Fig. 14 Thrust coefficient as a function of equivalence ratio for all fuel injection schemes.

Conclusions

An experimental study was presented for a scramjet engine with a rectangular-to-elliptical shape-transition inlet and an elliptical combustor at a simulated flight Mach number of 8.7 and a dynamic pressure of approximately 0.5 atm. The engine was designed to operate between Mach 6.0 and 12.0 using gaseous hydrogen as the fuel, with no ignition aids. The inlet was designed using a quasi-streamline-tracing method with a geometric contraction ratio of 6.61 and an internal contraction ratio of 2.26, and it was preceded by a short forebody. The combustor included a constant-height backward-facing step around its circumference, generating an area ratio of 1.24. This was followed by a constant-area and diverging section to an area ratio of 2.0 and, together with a short thrust nozzle, had a total area ratio of 8.0.

The engine was fueled in the experiments by four different fuel injection configurations to assess the overall performance in terms of thrust coefficient. These were intake injection, injection at the combustor step, and injection from both stations at two different relative proportions. Combustion was observed for all configurations at all fuel levels tested. With intake injection, combustion-induced pressure rise was measured within the isolator section between the inlet throat and the step, and the engine unstarted at equivalence ratios of 0.61 and above. For injection at the step, combustion occurred immediately downstream of the step and was clearly mixing-limited. Two combinations of intake and step injection were tested. Combustion occurred within the isolator at all equivalence ratios tested with a 9:11 ratio scheme. With the use of the combined 1:2 injector system, pressure rise in the isolator was reduced, while maintaining similar levels of thrust as the 9:11 combined injection scheme. Robust supersonic combustion took place for both combined injection systems up to an equivalence ratio of 1.23, and no inlet unstarts were observed. A key result of these experiments was the presence of good combustion at all conditions without the use of ignition aids, indicating the presence of robust fluid-dynamic flameholding regions.

For all injection configurations, estimation of the thrust coefficient indicated that a small amount of thrust was produced from mass addition alone. For all injection configurations, thrust-coefficient estimates as a result of combustion were positive at equivalence ratios of 0.3 and above. The thrust generated by combustion through intake injection was higher than measured levels from step injection at equivalence ratios below 0.41. At equivalence ratios higher than 0.5, plateauing thrust levels due to step injection indicated that combustion was mixing-limited. However at the midrange equivalence ratio of 0.63–0.66, step injection generated approximately 30% more thrust that either combined injection configuration. Principally as a result of higher mixing efficiencies, the combined injection schemes produced greater thrust than other configurations at equivalence ratios above 0.75. Estimates of thrust coefficient in which skin-friction reduction by boundary-layer combustion were accounted for indicated a possible increase in net thrust of as much as 50%, due to this phenomenon for the step-injection configuration.

The results of this study show that a REST scramjet engine designed to operate at Mach numbers of interest to access-to-space applications can function efficiently at offdesign conditions.

Acknowledgment

This research was supported by the Australian Research Council under grant DP0452374.

References

[1] Smart, M. K., and Ruf, E. G., "Free-Jet Testing of a REST Scramjet at Off-Design Conditions," 25th AIAA Aerodynamic Measurement Technology and Ground Testing Conference, AIAA Paper 2006-2955, June 2006.

[2] Stalker, R. J., Paull, A., Mee, D. J., Morgan, R. G., and Jacobs, P. A., "Scramjets and Shock Tunnels—The Queensland Experience," *Progress in Aerospace Sciences*, Vol. 41, No. 6, 2005, pp. 471–513. doi:10.1016/j.paerosci.2005.08.002

[3] Beck, W. H., Hannemann, K., and Weiland, M., "Modifications to the DLR High Enthalpy Shock Tunnel HEG for Measurements of Supersonic Combustion," 10th AIAA/NAL-NASDA-ISAS International Space Planes and Hypersonic Systems and Technologies Conference, AIAA Paper 2001-1860, Apr. 2001.

[4] Itoh, K., Ueda, S., Tanno, H., Komuro, T., and Sato, K., "Hypersonic Aerothermodynamic and Scramjet Research Using a High Enthalpy Shock Tunnel," *Shock Waves*, Vol. 12, No. 2, 2002, pp. 93–98. doi:10.1007/s00193-002-0147-0

[5] Rogers, R. C., Shih, A. T., and Hass, N. E., "Scramjet Development Tests Supporting the Mach 10 Flight of the X-43," 13th AIAA/CIRA International Space Planes and Hypersonic Systems and Technologies Conference, AIAA Paper 2005-3351, May 2005.

[6] McClinton, C. R., "X-43—Scramjet power breaks the hypersonic barrier Dryden Lectureship in Research for 2006," 44th AIAA Aerospace Sciences Meeting and Exhibit, AIAA Paper 2006-0001, Jan. 2006.

[7] Smart, M. K., "Design of Three-Dimensional Hypersonic Inlets with Rectangular-to-Elliptical Shape Transition," *Journal of Propulsion and Power*, Vol. 15, No. 3, 1999, pp. 408–416. doi:10.2514/2.5459

[8] McClinton, C. R., "The Effect of Injection Angle on the Interaction Between Sonic Secondary Jets and a Supersonic Free Stream," NASA TN D-6669, Feb. 1972.

[9] "NECURON® 651 Data Sheet," http://www.necumer.de/com/produkte/modellbau/documents/20071101NECURON651.pdf [retrieved 12 Dec. 2007].

[10] Stalker, R. J., "Recent Developments with Free Piston drivers," *17th International Symposium on Shock Waves and Shock Tubes*, Vol. 208, American Inst. of Physics, Melville, NY, July 1990, pp. 96–107.

[11] Smith, C. E., "The Starting Process in a Hypersonic Nozzle," *Journal of Fluid Mechanics*, Vol. 24, No. 4, 1966, 1966, pp. 625–640. doi:10.1017/S0022112066000880

[12] Felderman, E. J., "Heat Transfer and Shear Stress in the Shock-Induced Unsteady Boundary Layer on a Flat Plate," *AIAA Journal*, Vol. 6, No. 3, 1968, pp. 408–412. doi:10.2514/3.4514

[13] Davies, W., and Bernstein, L., "Heat Transfer and Transition to Turbulence in the Shock-Induced Boundary Layer on a Semi-Infinite Flat Plate," *Journal of Fluid Mechanics*, Vol. 36, No. 1, 1969, pp. 87–112. doi:10.1017/S0022112069001534

[14] East, R. A., Stalker, R. J., and Baird, J. P., "Measurements of Heat Transfer to a Flat Plate in a Dissociated High-Enthalpy Laminar Air Flow," *Journal of Fluid Mechanics*, Vol. 97, No. 4, 1980, pp. 673–699. doi:10.1017/S0022112080002753

[15] Skinner, K. A., "Mass Spectrometry in Shock Tunnel Experiments of Hypersonic Combustion," Ph.D. Thesis, Dept. of Mechanical Engineering, Univ. of Queensland, Brisbane, Australia, 1994.

[16] Paull, A., "A Simple Shock Tunnel Driver Gas Detector," *Shock Waves*, Vol. 6, No. 5, Nov. 1996, pp. 309–312.

[17] Lordi, J. A., Mates, R. E., and Moselle, J. R., "Computer Program for the Numerical Solution of Nonequilibrium Expansion of Reacting Gas Mixtures," NASA CR-472, May 1966.

[18] He, Y., and Morgan, R. G., "Transition of Compressible High Enthalpy Boundary Layer Flow over a Flat Plate," *The Aeronautical Journal*, Vol. 98, No. 972, 1994, pp. 25–34.

[19] White, J. A., and Morrison, J. H., "A Pseudo-Temporal Multi-Grid Relaxation Scheme for Solving the Parabolized Navier–Stokes Equations," 14th AIAA Computational Fluid Dynamics Conference, AIAA Paper 99-3360, 1999.

[20] Tanno, H., Paull, A., and Stalker, R. J., "Skin-Friction Measurement in a Supersonic Combustor with Crossflow Fuel Injection," *Journal of Propulsion and Power*, Vol. 17, No. 6, 2001, pp. 1333–1338. doi:10.2514/2.5883

[21] Goyne, C. P., Stalker, R. J., and Paull, A., "Shock-Tunnel Skin-Friction Measurement in a Supersonic Combustor," *Journal of Propulsion and Power*, Vol. 15, No. 5, 1999, pp. 699–705. doi:10.2514/2.5481

[22] McMurtry, P. A., Riley, J. J., and Metcalfe, R. W., "Effects of Heat Release on the Large-Scale Structure in Turbulent Mixing Layers," *Journal of Fluid Mechanics*, Vol. 199, 1989, pp. 297–332. doi:10.1017/S002211208900039X

[23] Stalker, R. J., "Control of Hypersonic Turbulent Skin Friction by Boundary-Layer Combustion of Hydrogen," *Journal of Spacecraft and Rockets*, Vol. 42, No. 4, 2005, pp. 577–587. doi:10.2514/1.8699

[24] Van Driest, E. R., "The Problem of Aerodynamic Heating," *Aeronautical Engineering Review*, Vol. 15, No. 10, Oct. 1956, pp. 26–41.

R. Bowersox
Associate Editor